Measurement of ^{17}F(d,n)^{18}Ne and the impact on the ^{17}F(p,γ)^{18}Ne reaction rate for astrophysics

S. A. Kuvin,* J. Belarge,† L. T. Baby, J. Baker, I. Wiedenhöver,‡ P. Höflich, and A. Volya
Physics Department, Florida State University, Tallahassee, Florida 32306, USA

J. C. Blackmon, C. M. Deibel, H. E. Gardiner, J. Lai, L. E. Linhardt, K. T. Macon, and B. C. Rasco
Department of Physics and Astronomy, Louisiana State University, Baton Rouge, Louisiana 70803, USA

N. Quails, K. Colbert, and D. L. Gay
Department of Physics, University of North Florida, Jacksonville, Florida 32224, USA

N. Keeley
National Centre for Nuclear Research, ul. Andrzeja Sołtana 7, 05-400 Otwock, Poland
(Received 30 April 2017; published 27 October 2017)

Background: The ^{17}F(p,γ)^{18}Ne reaction is part of the astrophysical "hot CNO" cycles that are important in astrophysical environments like novas. Its thermal reaction rate is low owing to the relatively high energy of the resonances and therefore is dominated by direct, nonresonant capture in stellar environments at temperatures below 0.4 GK.
Purpose: An experimental method is established to extract the proton strength to bound and unbound states in experiments with radioactive ion beams and to determine the parameters of direct and resonant capture in the ^{17}F(p,γ)^{18}Ne reaction.
Method: The ^{17}F(d,n)^{18}Ne reaction is measured in inverse kinematics using a beam of the short-lived isotope ^{17}F and a compact setup of neutron, proton, γ-ray, and heavy-ion detectors called RESONEUT.
Results: The spectroscopic factors for the lowest $l = 0$ proton resonances at $E_{c.m.} = 0.60$ and 1.17 MeV are determined, yielding results consistent within 1.4σ of previous proton elastic-scattering measurements. The asymptotic normalization coefficients of the bound 2_1^+ and 2_2^+ states in ^{18}Ne are determined and the resulting direct-capture reaction rates are extracted.
Conclusions: The direct-capture component of the ^{17}F(p,γ)^{18}Ne reaction is determined for the first time from experimental data on ^{18}Ne.

DOI: 10.1103/PhysRevC.96.045812

I. INTRODUCTION

Steady-state hydrogen burning in stellar environments can proceed in several reaction sequences, all of which convert protons to helium nuclei. For main-sequence massive stars "cold CNO" cycles dominate energy production, which proceeds in cyclical sequences of (p,γ), β^+ decay, and (p,α) reactions on the preexisting carbon, nitrogen, and oxygen seed nuclei. "Hot CNO" cycles become significant at temperatures typical for nova outbursts, in which hydrogen-rich material is accreted onto a white dwarf in a close binary system. As nuclear reactions release energy and increase the temperature, (p,γ) reactions become competitive with β^+-decay half-lives and wider reaction cycles open up, which involve short-lived isotopes and thus help accelerate the energy generation into a thermonuclear runaway. A review of the nuclear reactions comprising CNO cycles and their role in astrophysics has been given in Ref. [1].

The rate of the ^{17}F(p,γ)^{18}Ne reaction determines the temperature and density conditions under which the slow ^{17}F β decay is bypassed, which increases energy generation and affects the isotopes produced in explosions like novas. At temperatures higher than 0.4 GK, breakout paths to the rp process become significant, including the reaction ^{18}Ne(α,p)^{21}Na, which occurs in sequence with the ^{17}F(p,γ)^{18}Ne reaction. The corresponding reaction rates influence the temperature conditions and time scale for breakout from the hot CNO cycles, relevant for environments like x-ray bursts.

The most important information for the determination of astrophysical (p,γ)-reaction rates is whether there are resonances in the relevant energy range, at what energies they are located, and what quantum numbers they possess. In the case of ^{17}F(p,γ)^{18}Ne, this information was initially investigated through stable-beam transfer experiments, such as (^{3}He,n) [2] and (p,t) [3,4]. However, these studies were not able to identify the most important 3^+, $l = 0$ proton resonance, which was expected to exist from the excitation spectrum of the analogous mirror nucleus ^{18}O.

Only when experiments with the radioactive isotope ^{17}F became possible could the resonance structure of ^{18}Ne be firmly established, with the 3^+ resonance at 599.8-keV c.m. energy, observed in proton elastic scattering [5,6] and, later, by measuring the (p,γ) reaction strength to this resonance

*Current address: Physics Department, University of Connecticut, Mansfield, Connecticut 06269.
†Currently an MIT Lincoln Laboratory employee. No Laboratory funding or resources were used to produce the results/findings reported in this publication.
‡iwiedenhover@physics.fsu.edu

directly [7]. These measurements established the 599.8-keV resonance to be the dominant path of resonant proton capture, with the two other narrow resonances, the 1^-, $l = 1$ resonance at 597 keV and the 0^+, $l = 2$ resonance at 665 keV, providing much smaller contributions. Because of their relatively high excitation energies, none of these resonances contributes substantially to the overall reaction rate for temperatures below 0.4 GK. In the absence of additional lower-lying resonances, the reactions at temperatures typical for nova explosions are dominated by the nonresonant "direct-capture" mechanism for (p,γ) reactions.

At this time it is still impossible to measure the associated direct-capture (p,γ) cross sections at astrophysical energies in experiments involving short-lived radioactive isotopes, and it will remain difficult even with the next generation of radioactive-beam facilities. As a consequence, there is a need to develop reliable alternative methods to obtain the relevant spectroscopic information needed to determine astrophysical reaction rates. The (d,n) proton-transfer reaction is well suited to populate the pertinent low-angular-momentum states and resonances around the proton-binding threshold, owing to its low-magnitude Q value of -2.2 MeV at the threshold and the simple transfer mechanism compared to alternative reactions. However, since significant experimental difficulty is involved in neutron detection, few attempts have been made to perform spectroscopy with the (d,n) reaction and radioactive ion beams.

In the past our group has used the (d,n) reaction in inverse kinematics to populate proton resonances of astrophysical interest, relying on the proton emission from these resonances. The high sensitivity of this approach was demonstrated in studies of the low-lying proton resonances of ^{26}Si [8,9] through the ^{25}Al$(d,n)^{26}$Si reaction. In a similar approach the ^{18}F$(d,n)^{19}$Ne reaction [10] was studied at Oak Ridge National Laboratory. A more recent application, using the same experimental setup as in the present work, was described in a study of the ^{19}Ne$(d,n)^{20}$Na reaction, which identified the angular momentum quantum numbers of the resonance spectrum and, for the first time, quantified a (p,γ) reaction rate proceeding from an excited initial state based on experimental information [11].

The present work describes the first successful experiment using neutron time-of-flight (tof) spectroscopy with the (d,n) reaction on a radioactive ion beam. In the following sections we briefly describe the experimental setup, the design and performance characteristics of the neutron-detector system, the analysis techniques for proton-decaying and γ-decaying excitations of ^{18}Ne, the results obtained, and their impact on the astrophysical reaction rate of ^{17}F$(p,\gamma)^{18}$Ne. A more detailed description of the experimental setup, with a focus on the neutron-detector systems, performance characterization, and calibration procedures, has been given in Ref. [12].

II. EXPERIMENT

A beam of ^{17}F was produced in-flight through the ^{16}O$(d,n)^{17}$F reaction with a beam of ^{16}O bombarding a gas cell containing deuterium gas. The beam of ^{17}F reaction residues was separated by means of the RESOLUT radioactive ion beam facility [13] at the John D. Fox Accelerator Laboratory of Florida State University. The ^{17}F beam was focused onto a deuterated polyethylene (CD_2) target foil with a thickness of 520 μg/cm^2 located at the center of a compact detector system. A beam energy of 95.5 MeV, an average beam intensity of 2.8×10^4 ^{17}F per second, and a purity of 60% were maintained throughout the experiment.

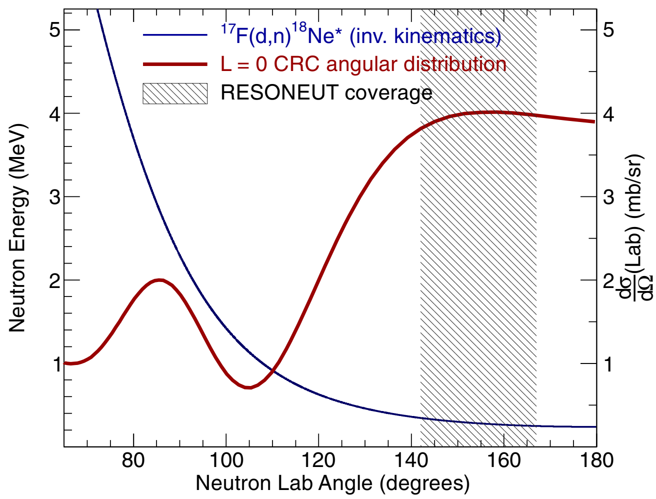

FIG. 1. Angular kinematics and angular distribution for an $l = 0$ proton transfer for the ^{17}F$(d,n)^{18}$Ne* reaction in inverse kinematics, populating a state at 4.5-MeV excitation energy. The primary y axis and thin-solid-line graph represent the neutron energy, and the secondary y axis and thick-solid-line graph represent the differential cross section in the laboratory system, as predicted by a coupled-reaction-channel (CRC) calculation.

The design of the detection system and, in particular, the neutron detectors was optimized to match the kinematic conditions for populating low-lying resonances with (d,n) reactions in inverse kinematics, i.e., with a heavier beam bombarding deuterium nuclei. As shown in Fig. 1, the neutron angular distributions for low-angular-momentum proton-transfer reactions are predominantly forward peaked in the center-of-mass (c.m.) system and thus backward peaked in the laboratory system for inverse-kinematics reactions. These events also possess low energies, as displayed in Fig. 1. Thus, a relatively compact setup of neutron detectors placed upstream from the target and capable of detecting low-energy neutrons will have a good efficiency for the events of interest. A sketch of the experimental apparatus is shown in Fig. 2.

A. The resoneut compact neutron detector array

For the kinematics of our experiment, (d,n) neutrons are emitted at energies between 100 and 600 keV, which requires the use of neutron detectors with very low energy-detection thresholds. The parameters of the entire detection system were investigated through a Monte Carlo simulation of the particle interactions with the detector and housing materials. Further details on the instrument design and data acquisition electronics, as well as the commissioning and performance characteristics of the neutron-detector systems and the simulation of the detector response, are described in Ref. [12].

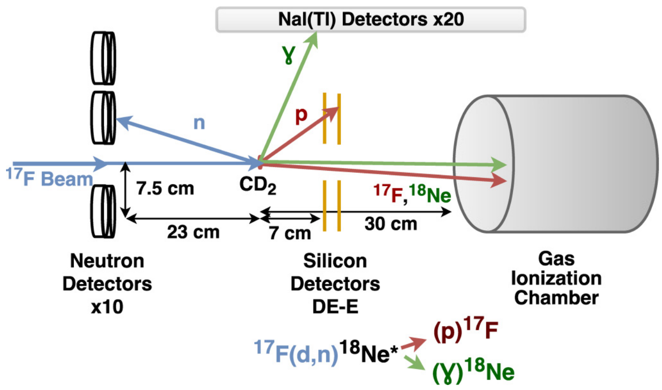

FIG. 2. Schematic of the experimental setup for the ^{17}F$(d,n)^{18}$Ne radioactive-beam experiment.

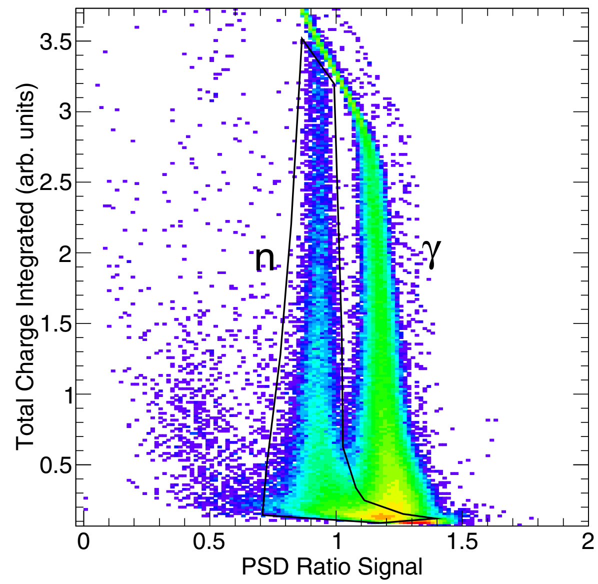

FIG. 3. Neutron pulse-shape discrimination spectrum for a single RESONEUT detector, representing γ^{-2} and neutrons emitted from a ^{252}Cf source. Also drawn is the gate used to select neutron-based events in the analysis.

The scintillation material *p*-terphenyl was chosen for its high light output as well as its ability to discriminate between neutron- and γ-induced events. Neutrons are detected through their elastic scattering with the hydrogen in the scintillator material, while γ's interact with the electrons, leading to different ionization densities and different scintillation-time parameters, which can be distinguished through pulse-shape analysis. The scintillation crystals, fabricated by Cryos-Beta Ltd. in Ukraine, were coupled to Planacon photomultipliers by Photonis Inc. These multipliers employ microchannel plates to produce signals with excellent timing, matched to the very fast pulses of the *p*-terphenyl scintillators. The neutron-detector systems were placed along a plane perpendicular to the beam axis at a distance 23.1 cm upstream from the target, covering an angular range of 3°–10° in the c.m. frame. Three crystals of 1.25-cm thickness were placed closer to the beam axis and seven crystals of 2.5-cm thickness were placed around them.

The detector pulse shapes are analyzed through a gated-integration technique, which separates γ- from neutron-induced events above 50- to 60-keV electron-equivalent energies, as shown in Fig. 3. In order to characterize the threshold and detection efficiencies, a series of calibration experiments with a ^{252}Cf fission source and an in-beam experiment with the ^{12}C$(d,n)^{13}$N reaction were performed, employing the same experimental setup. The region of pulse-shape parameters to select neutron events, represented in Fig. 3, was drawn to conserve any neutron signals while suppressing clearly identified γ rays. While neutron and γ rays cannot be separated at the lowest energies, relevant events are selected through the coincident detection of the reaction residue and a proton or a γ ray, as described in the following sections. We obtained neutron-detection thresholds between 60 and 100 keV for the individual detectors and peak intrinsic detection efficiencies of 55% in the 2.5-cm-thick detectors and 30% in the 1.25-cm-thick detectors.

B. Other detector systems

The compact charged-particle detection system consisted of an annular silicon-strip detector telescope and gas ionization detector. Thin (65-μm) and thick (1000-μm) double-sided silicon strip detectors covered angles in the laboratory frame from 8° to 21° for detection of protons. Protons were identified according to their characteristic energy losses in the silicon detectors.

The gas ionization detector measures the parameters of the reaction-residue heavy ions in coincidence with the other particles and is placed 300 mm downstream from the target position. The detector consists of nine 4-cm-long cathode-anode-cathode ionization regions, with the drift directions along the beam axis. The short distance between each anode-cathode pairing allows for a short collection time and improved tolerance for high incident particle rates. The first two segments are fitted with position-sensitive anode grids consisting of 32 wires that are spaced 3 mm apart, providing a position sensitivity in the x and y dimensions, respectively. The following two sections measure the differential energy loss (dE) and the final five segments measure the remaining particle energy. In combination, the position-sensing, energy-loss, and total energy measurements allow for event-by-event tracking and Z identification of the beam particles or reaction residues. Further details on the design of the gas ionization detector will be given in Ref. [14].

In order to detect γ rays in coincidence, we use an array of 20 position-sensitive NaI(Tl) detectors arranged in a barrel formation around the vacuum chamber and the target. These detectors were originally part of the ATLAS Positron Experiment (APEX) [15] and were later used in radioactive ion beam experiments [16]. Owing to the geometric constraints of our setup the barrel was centered slightly downstream from the target position, resulting in a reduced angular coverage at backward angles.

The NaI(Tl) detector efficiency was calibrated using a ^{60}Co source through the detection of the 1.172- or 1.332-MeV γ rays. The absolute detection efficiency, for 1.25-MeV γ rays, was determined to be 12(1)% and this value was used to verify

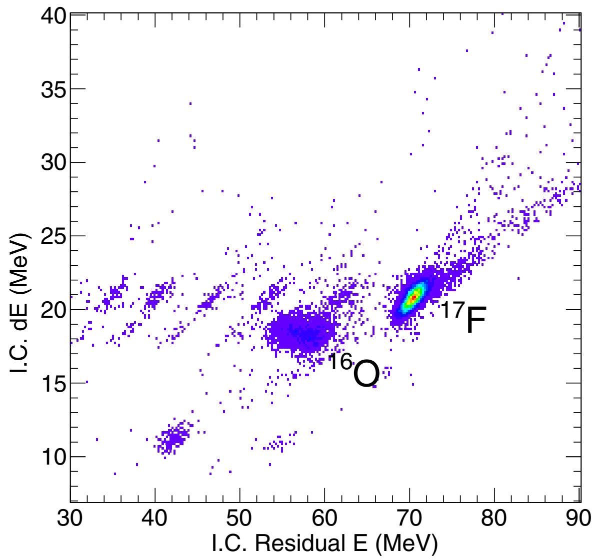

FIG. 4. Sample beam composition observed in the gas ionization chamber, characterized according to the partial energy loss (dE) and residual energy E detected in the active sectors of the chamber but excluding the position-resolving sections. This spectrum represents data taken without the CD_2 target. During the experiment the beam composition was continuously sampled at a 1/1000 downscaled trigger rate.

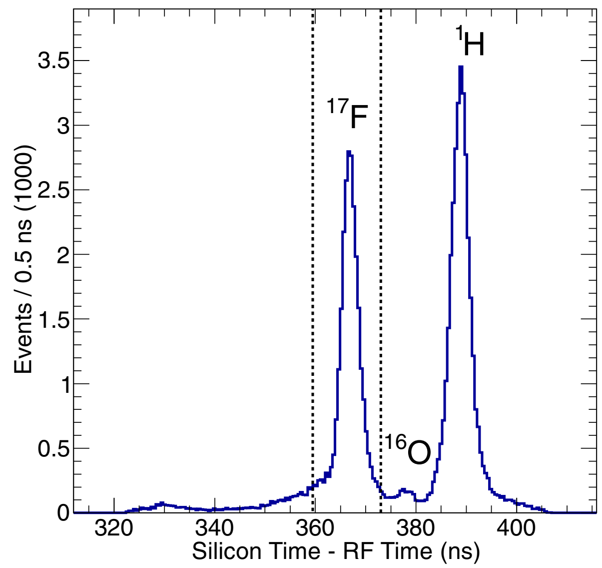

FIG. 5. Beam time-of-flight signal, measured between the silicon time signal and the accelerator RF reference signal. Contaminant ^{16}O and ^{1}H (proton) beam particles are identified in addition to the ^{17}F beam of interest. Protons are created in reactions at the production target, selected at the same rigidity as the beam, and can strike the inner rings of the silicon detector. The gate on ^{17}F events is shown, which was used for beam identification in the subsequent analysis.

a Monte Carlo simulation of the setup using the GEANT4 package, which was used to extrapolate the detection efficiency to other energies.

C. Event types and trigger conditions

Our experiment employed the ^{17}F$(d,n)^{18}$Ne reaction in inverse kinematics to populate excited states in ^{18}Ne and establish the spectrum of near-threshold states and low-lying resonances. When ^{18}Ne is produced in a proton-resonant state and decays by proton emission, both the proton and the resulting ^{17}F particle are emitted in forward directions, where they are detected in coincidence with a high efficiency. For these events, the 1000-μm-thick silicon detector provides the only required trigger condition.

In cases where an excited ^{18}Ne state decays through γ emission, the cascade of γ rays can be observed in the NaI detector barrel in coincidence with the heavy ion in the zero-degree gas ionization chamber. These events will also be distinguished through the characteristic energy-loss signals of the ^{18}Ne reaction residue. To record these events, a coincidence condition between a neutron detector and a NaI detector was used as a trigger in addition to the silicon-detector events. The total integrated ^{17}F beam intensity was determined by a downscaled trigger from the gas ionization detector, which also allows the ratio of the incident ^{17}F secondary beam to the contaminant ^{16}O to be monitored, as shown in Fig. 4.

In addition to the parameters of the detector systems, the time of the trigger relative to the accelerator radio frequency (rf) reference was recorded. This timing signal is used to suppress the contaminant components in the beam, as shown in Fig. 5, and as a reference for neutron time-of-flight measurements.

III. SPECTROSCOPY OF LOW-LYING PROTON RESONANCES

A. Analysis of proton spectra

For excited states of ^{18}Ne at energies high enough above the proton threshold, proton emission dominates over γ emission and the decay protons can be used for efficient resonance spectroscopy. This is the case for all known proton resonances in ^{18}Ne. Experimentally, the protons are identified through their stopping power signature, as shown in Fig. 6. Figure 7 displays the spectrum of recoiling heavy ions detected in coincidence with protons. Although some of the ^{17}F unreacted-beam particles are present in the spectrum as an effect of random coincidences, the ^{17}F reaction residues are cleanly separated by their lower energy.

The excitation energies of the $p + {}^{17}$F coincident events were reconstructed through an invariant mass analysis of the ^{18}Ne compound system, using the detection angles and energies of the charged particles. The resulting spectrum of the c.m. resonance energies is shown in Fig. 8. Two peaks are observed, at 0.60 and 1.16 MeV, consistent with the previously identified 3^+ resonance at 0.5998 MeV and the previously identified 2^+ resonance at 1.165 MeV. Since these are located well above the proton separation threshold, it is safe to assume that they decay exclusively by proton emission in determining the cross section. We extract total cross sections of $15.3^{\pm 0.3\,\text{stat.}}_{\pm 1.2\,\text{syst.}}$ and $2.3^{\pm 0.35\,\text{stat.}}_{\pm 0.29\,\text{syst.}}$ mb for populating the states at 0.60 and 1.16 MeV, respectively. The systematic errors encompass the

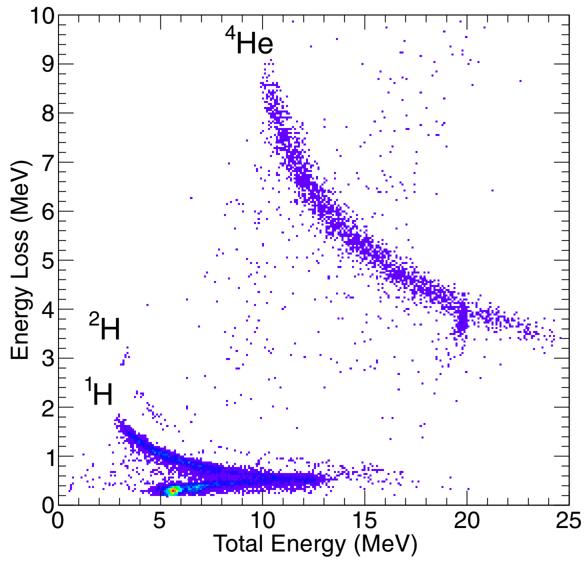

FIG. 6. Light charged particles identified in the $\Delta E - E$ silicon detectors according to their characteristic energy losses and selected by gating on incident ^{17}F beam particles, identified through the time-of-flight analysis displayed in Fig. 5.

uncertainties of the target thickness, the detector geometry, and the number of incoming beam particles.

B. Analysis of unobserved-neutron kinematics

In the analysis described so far and in this section, neutrons from the (d,n) reaction remained unanalyzed, making use

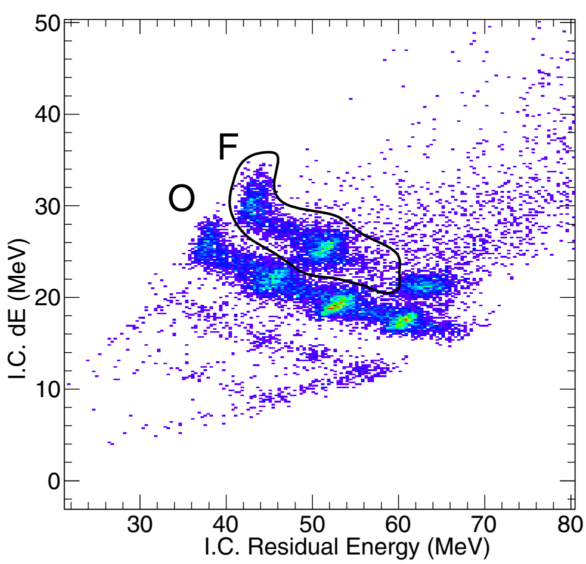

FIG. 7. Heavy-ion particles identified in the gas ionization chamber according to their characteristic energy losses, with the signals equivalent to those in Fig. 4. Events were selected by gating on incident ^{17}F beam particles (see Fig. 5) and a coincident proton. A gate is drawn identifying the ^{17}F reaction products. Note that the peak around 50-MeV energy corresponds to the strong, 0.6-MeV proton resonance observed in this experiment.

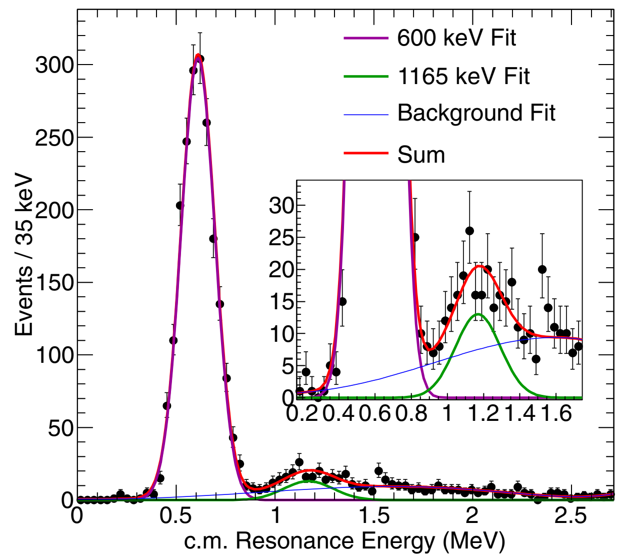

FIG. 8. Center-of-mass resonance-energy spectrum reconstructed from the invariant-mass analysis of the detected coincident proton + ^{17}F events. The spectrum is dominated by a peak at 0.60 MeV. Inset: Energy spectrum expanded in the region of the state expected at 5.09 MeV. Both spectra show a fit hypothesis of the two resonance peaks and a polynomial background.

of the highly efficient charged-particle detection with silicon detectors and the gas ionization chamber alone. Since the complete ^{17}F$(d,n)^{18}$Ne$(p)^{17}$F reaction path amounts to the disintegration of a deuteron, the overall Q value is -2.22 MeV. This also implies that the sum energy of the detected reaction products is a direct function of the unobserved neutron energy, with $(E^{17}\text{F}) + E(p) = E_{\text{Beam}} - E(n) - 2.22$ MeV. In the inverse kinematics of our experiment, the neutron energy exhibits a rapid kinematic variation as a function of the emission angle, which has the effect of creating an imprint of the neutron angular distribution in the summed energies of the ^{17}F and the proton. This correlation of detected charged-particle energy and center-of-mass neutron emission angle is illustrated in Figs. 9(a) and 9(b), which shows the results of a Monte Carlo simulation for the $E(^{17}\text{F}) + E(p)$, as it depends on the c.m. neutron angles.

The angular distributions are deduced from a coupled-reaction-channel (CRC) calculation performed with the code FRESCO [19]. The entrance channel optical potential was obtained by a Watanabe-type folding of the global parameters of Koning and Delaroche [20] over a deuteron internal wave function calculated with the Reid soft-core interaction [21]. Deuteron breakup was explicitly taken into account via the coupled-discretized-continuum-channels technique [22,23]. The exit channel optical potential was calculated using the Koning and Delaroche parameters. The proton was bound to the ^{17}F core in a Woods-Saxon potential well of radius $R_o = 1.25 \times A^{\frac{1}{3}}$ fm and diffuseness $a = 0.65$ fm. The well depth was adjusted so that the resonances are treated as being just barely bound at 0.01 MeV and with a spin-orbit term of the same geometry and a fixed depth of 6.0 MeV. This "weak-binding" approximation treats these low-lying

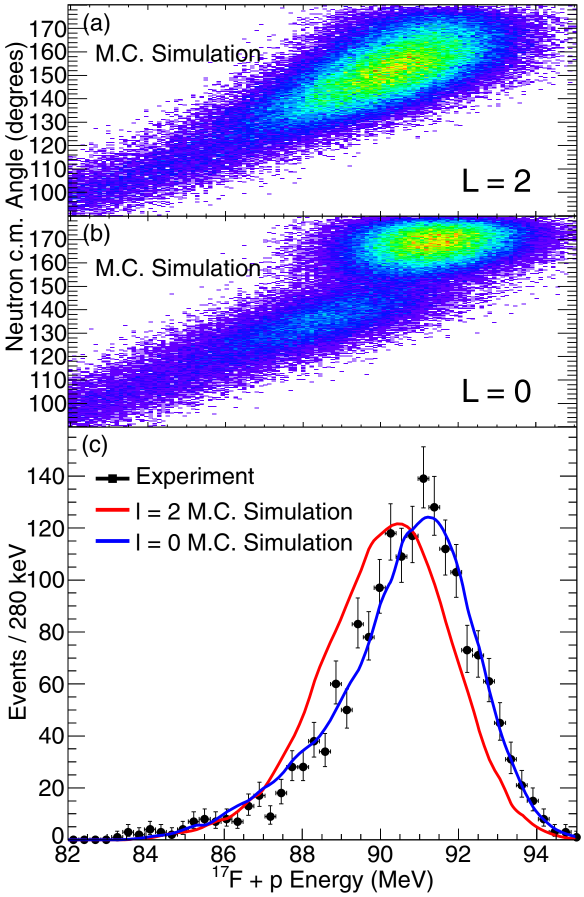

FIG. 9. The ^{17}F + p energy distribution for the state at 4.5 MeV is fit with the simulated spectrum assuming that the state is populated by either $l = 0$ or $l = 2$ proton transfer.

resonances as being quasibound, a justified approximation when applied to these relatively sharp resonances.

The experimental summed energies of the charged reaction products from the population of the 0.60-MeV resonance are shown in Fig. 9(c). In addition to the experimental data, the Monte Carlo simulations corresponding to two angular momentum hypotheses are shown. The experimental resolution of the correlation between neutron angle and summed energy is dominated by the ≈ 1-MeV energy resolution of the gas ionization detector, which was determined from the signals of the detected ^{17}F beam particles. The simulated distribution for $l = 0$ reproduces the data well, while the $l = 2$ distribution does not. This analysis provides independent confirmation that the 0.60-MeV resonance is of $l = 0$ character and supports the 3^+ assignment [5]. While no contrasting $l = 2$ distribution was observed in the present experiment, a recent work studying the ^{19}Ne(d,n)^{20}Na reaction with the same setup and analysis method observed resonances matching both $l = 2$ and $l = 0$ distributions [11].

The analysis described above provides a sensitive method with which to analyze angular momentum properties of the transfer reaction from unobserved neutron energies. A similar approach has been described by Adekola *et al.* in Ref. [10], where the unobserved neutron angle in the ^{18}F(d,n)^{19}Ne was reconstructed from the charged particle residues, which was possible because of the high beam quality available at the HRIBF facility. By contrast, the RESOLUT in-flight facility delivers beams with poor transverse emittance, which does not allow analysis of the heavy-ion scattering angles, but a sufficiently defined beam energy, which allows for analysis of the missing-energy spectra. Note that the analysis presented above was limited by the ion-chamber energy resolution, not the beam energy definition.

The results from the analysis of the proton-based events are summarized in Table I. Spectroscopic factors are obtained as scaling factors of the measured cross sections relative to the CRC-calculated cross sections. For the dominant 3^+ resonance a spectroscopic factor of $0.78^{\pm 0.02\,\text{stat.}}_{\pm 0.06\,\text{syst.}}$ is extracted, which compares to the value of 1.01 measured in the mirror reaction ^{17}O(d,p)^{18}O in Ref. [17]. The other observed resonance, at 1.165 MeV, is identified with a 2^+ state, consistent with the assignment in Ref. [6] and consistent with the respective spectroscopic factor obtained in the mirror reaction [17]. This agreement also excludes the assignment of 3^- to this state, as a mirror to the ^{18}O state at 5.090 MeV, which would be energetically possible but would lead to a much smaller spectroscopic factor and a cross section too small to be observed in our experiment. The systematic errors quoted for spectroscopic factors are based on the cross-section determination; no error was added for the uncertainties of the CRC calculation parameters.

The extracted spectroscopic factors were also used to calculate the proton-width parameters for the observed resonances. To this effect, the single-particle proton widths were calculated as a barrier penetration probability in a Woods-Saxon potential of the same geometry as that used in the CRC calculation. The resonance proton widths were then

TABLE I. Summary of the known ^{17}F + p resonances, up to $E^R_{\text{c.m.}} = 1.2$ MeV, in ^{18}Ne. Spectroscopic factors extracted in this experiment are compared with the spectroscopic factors obtained from the mirror reaction [17]. The proton widths deduced from our experiment are compared with results from proton elastic scattering experiments [2,5,18].

Adopted values			This work			Previous work		
E_x (MeV)	$E_R^{\text{c.m.}}$ (keV)	J^π	$\sigma^{\text{stat.}}_{\text{syst.}}$ (mb)	$C^2S^{\text{stat.}}_{\text{syst.}}$	$\Gamma_p{}^{\text{stat.}}_{\text{syst.}}$ (keV)	Mirror C^2S [17]	Γ_p (keV) [2,5,18]	Γ_γ (meV) [2,7]
4.519	597	1^-	–	–	–	0.03	9 ± 6	15 ± 3
4.523	599.8	3^+	$15.3^{\pm 0.3}_{\pm 1.2}$	$0.78^{\pm 0.02}_{\pm 0.06}$	$14.2^{\pm 0.3}_{\pm 1.1}$	1.01	18 ± 2	56 ± 38
4.590	665	0^+	–	–	–	0.16	4 ± 4	1.0 ± 2
5.09	1165	2^+	$2.3^{\pm 0.35}_{\pm 0.29}$	$0.20^{\pm 0.03}_{\pm 0.03}$	$50^{\pm 8}_{\pm 8}$	0.35	42 ± 4	–

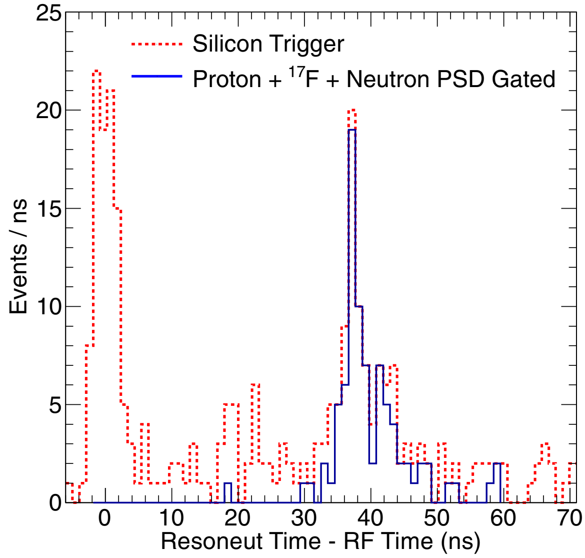

FIG. 10. Time-of-flight (tof) signals of neutron detection analyzed relative to the accelerator RF reference for ^{17}F-based events triggered by a silicon detector. Shown is the raw distribution, including the γ-based events at 0.6-ns tof and the events detected in coincidence with an identified proton, a heavy ion, and applied γ discrimination through the pulse-shape analysis.

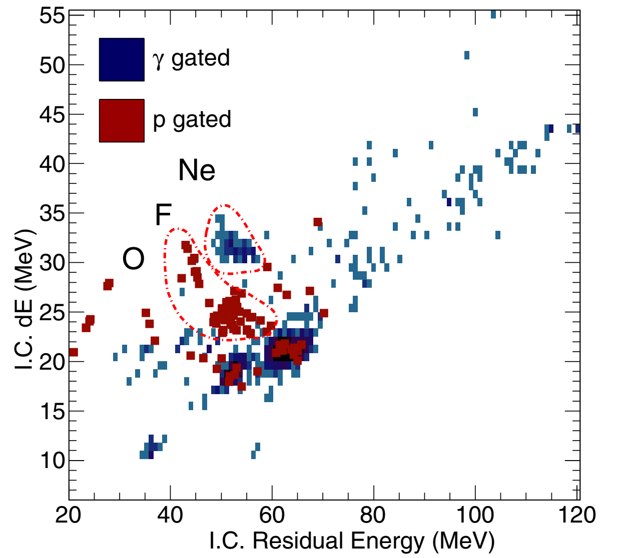

FIG. 11. Energy loss and residual energy detected in segments of the gas ionization chamber, equivalent to those displayed in Fig. 4 and Fig. 7, selected for neutron-γ coincidence events (blue symbols) and neutron-proton coincidence events (red symbols). A separation between $Z = 9$ and $Z = 10$ regions is obtained in the reaction residues marked by the dashed-line regions. Separated at higher energies, the spectrum also contains background events from random coincidences with beam particles of ^{17}F and ^{16}O and beam-particle pileup events.

obtained by multiplying the single-particle decay width with the spectroscopic factors listed in Table I. The deduced widths differ by only slightly more than 1σ compared with the proton widths determined experimentally in proton elastic scattering experiments [5,6].

C. Analysis of neutron spectra

The neutron-spectroscopy component of the present experiment can provide additional information, in particular, on bound states and on potential lower-lying resonances, which may decay by γ emission. We start by analyzing the neutrons detected in coincidence with a proton emitted from a populated resonance. This type of event was used to develop the(tof spectroscopy analysis, both from the present $^{17}F(d,n)^{18}Ne(p)^{17}F$ reaction and from a series of test experiments with the stable beam reaction $^{12}C(d,n)^{13}N(p)^{12}C$, which is discussed in Ref. [12] in more detail. The neutron tof is analyzed through the time difference between the accelerator-rf reference and the neutron-detector time signal. The values of this parameter are independent of the trigger condition and thus can be applied to all events involving neutrons. The zero point of the tof spectra was determined through γ-ray signals detected in the p-terphenyl detectors. The spectrum location of this reference was evaluated for individual data runs recorded throughout the experiment in order to correct for shifts of up to 1.5 ns in the ^{17}F arrival times.

The resulting time-of-flight spectrum is displayed in Fig. 10. The dashed-line histogram shows the tof parameter for all events triggered by a silicon detector, showing γ detection events around 0.6 ns, the expected γ tof. The solid-line histogram shows the effect of gating on proton-recoil coincidences and the neutron pulse shapes. A peak is observed in the tof spectrum at approximately 37 ns, which is the time of flight expected for populating the resonance at 598-keV c.m. energy.

The reconstructed excitation energy spectrum based on the neutron-tof signals and the associated resonance energy is displayed in Fig. 12(a), with the spectrum dominated by the 3^+ state at 598-keV c.m. resonance energy, with a resolution of 150-keV FWHM (c.m.). The observed cross section for the 598-keV resonance is $41^{\pm 5\,\text{stat.}}_{\pm 5\,\text{syst.}}$ mb/sr at 6° in the c.m. system. From this value and the CRC calculation a spectroscopic factor of $0.84^{\pm 0.1\,\text{stat.}}_{\pm 0.1\,\text{syst.}}$ is extracted, consistent with the value $0.78^{\pm 0.02\,\text{stat.}}_{\pm 0.06\,\text{syst.}}$ extracted from the proton-decay cross section. This result is an independent verification of the applied analysis methods. The neutron yield expected from the 2^+ resonance at 1.17 MeV was below the sensitivity of the experiment.

The above-described reconstruction of excitation energies from neutron times of flight also allows us to study the bound-state spectrum using the same analysis methods. However, lean identification of the $^{17}F(d,n)^{18}Ne + \gamma$ events over the background of environmental radiation is more difficult here, since the final-state particles are neutral with the exception of the ^{18}Ne reaction residue. In addition, clean identification of ^{18}Ne particles in the gas ionization chamber was affected by the significant background of pileup events, from the high rate of incident $Z = 9$ beam particles. A sufficient reduction in this background was achieved by suppression of events with more than one ionization locus or inconsistent values in the three ΔE signals. The resulting $\Delta E - E$ spectrum observed in the gas ionization chamber, separated for γ-gated and proton-gated

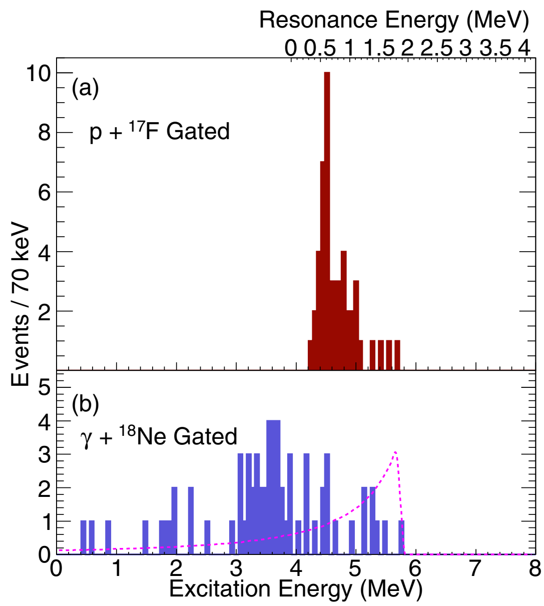

FIG. 12. Excitation energies of states populated by the (d,n) reaction reconstructed using the neutron time-of-flight measurement (see text). (a) Events detected in coincidence with a proton and a ^{17}F reaction residue. (b) Events detected in coincidence with a γ-ray and a ^{18}Ne reaction residue. The dashed line in (b) represents an upper-limit estimate for events from uncorrelated background in the time spectra.

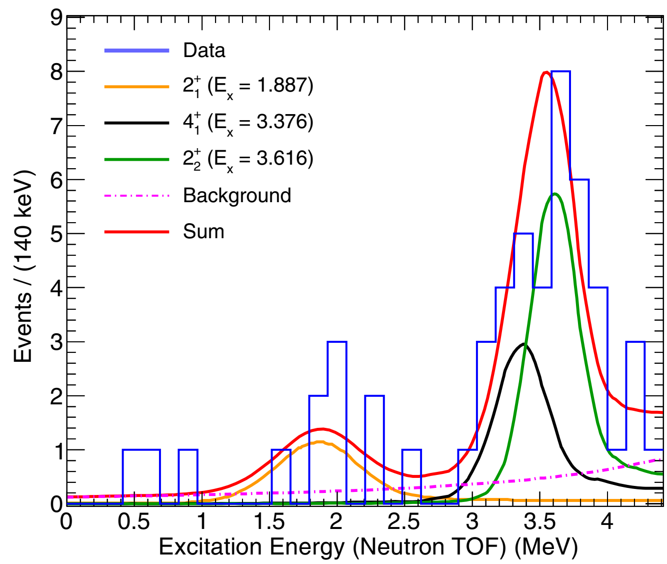

FIG. 13. The observed spectrum compared with three peaks at the locations of ^{18}Ne bound states 2_1^+, 4_1^+, and 2_2^+. Peak areas are consistent with expectations from the simulation based on spectroscopic factors from the mirror reaction [17].

events, is displayed in Fig. 11. The spectrum shows a clearly separated region of $Z = 10$ neon reaction residues, which in turn were selected to produce the neutron time-of-flight spectra for the γ-decaying ^{18}Ne states.

The resulting excitation-energy spectrum is displayed in Fig. 12(b). A clear separation of the γ-coincidence events from the proton-coincidence events [displayed in Fig. 12(a)] is achieved. For these events, an energy-dependent background estimate is also displayed, derived from the rate of uncorrelated, random events. The observed events show signals of bound-state population but no evidence of γ decays from unbound states.

An expanded view of the same spectrum from γ-coincident events is shown in Fig. 13. We observe peaks corresponding to the 2_1^+ state at 1.9 MeV and a doublet of the 2_2^+ and 4_1^+ states around ≈ 3.5 MeV. A third state located around that energy, the $l = 2$ 0_2^+ state, is expected to be populated much more weakly than the 4_1^+ and was thus omitted from our analysis. Although the 4_1^+ state dominates the total transfer-reaction cross section through its substantial $l = 2$ transfer, the detector angles of RESONEUT create a strong detection bias for peripheral reactions and $l = 0$ transfers, which enhances the 2_2^+ state, with its strong $l = 0$ component, over the 4_1^+. This is advantageous for determining the astrophysical reaction rate since direct capture to the 4_1^+ state is suppressed due to the low penetrability of $l = 2$ protons at low energy. The spectrum was fit using the Monte Carlo simulation of the setup, including effects of the peak shape and detection efficiency.

The efficiency of coincident γ and neutron detection was determined using the Monte Carlo simulation, based on information from the literature [24] for the corresponding γ-ray energies and branching ratios. Cascade transitions such as $3.616 \rightarrow 1.887 \rightarrow 0$ and $3.376 \rightarrow 1.887 \rightarrow 0$ are also modeled, resulting in an increase in the detection efficiency for the 4_1^+ and 2_2^+ states over the 2_1^+ state.

The resulting cross sections for the bound states, along with the 598-keV resonance, are listed in Table II. The extracted spectroscopic factors are consistent with those from the mirror reaction ^{17}O$(d,p)^{18}$O [17]. However, because of the low statistics and the small angular coverage of the neutron detectors, it was not possible to independently obtain the relative contributions of $l = 0$ and $l = 2$ components to the 2^+ states.

Since our experiment's detection efficiency only varies slowly with the excitation energy, the observed spectrum also allows us to establish upper limits for the spectroscopic factors of potential additional low-lying resonances. We estimate an upper limit of $C^2S \leqslant 0.10$.

D. Extraction of asymptotic normalization coefficients

The difficulty in measuring the small cross section associated with direct-capture (p,γ) reactions on radioactive isotopes is discussed in Sec. I. As an alternative method, the asymptotic normalization coefficients (ANCs) associated with the bound states of the final nucleus have been analyzed to derive the direct-capture cross sections relevant to astrophysical processes, a method that has seen increasing application. A review of this method and related approaches by Tribble *et al.* was recently published [26].

ANCs are a measure of the exterior of the nuclear wave function as sampled through the cross sections of peripheral transfer reactions. The formalism has also been shown to be largely independent of specifics of the chosen optical potentials. Prior investigations of the direct proton capture rate in ^{17}F$(p,\gamma)^{18}$Ne have relied on the extracted ANCs from

TABLE II. Summary of the known bound states in ^{18}Ne. Spectroscopic factors extracted from the analysis of observed neutron events are compared with the spectroscopic factors obtained from the mirror reaction [17]. Asymptotic normalization coefficients are extracted in a manner similar to the spectroscopic factors and compared with the ANCs obtained indirectly from Ref. [25], which were extracted by applying mirror symmetry.

Adopted values			This work					Previous work	
E_x (MeV)	J^π	nlj	$\frac{d\sigma}{d\Omega}{}^{\text{stat.}}_{\text{syst.}}$ ($\frac{mb}{sr}$)	$\theta_{\text{c.m.}}$ (deg)	$C^2S^{\text{stat.}\,a}_{\text{syst.}}$	ANC$^{\text{stat.}}_{\text{syst.}}$ C^2_{lj} (fm^{-1})[a]	ANC$^{\text{stat.}}_{\text{syst.}}$ C^2_{lj} (fm^{-1})[b]	Mirror C^2S [17]	ANC C^2_{lj} [25] (fm^{-1})
0	0^+	$1d5/2$			–	–	–	1.22	12.2 ± 1.2
1.888	2^+	$2s1/2$	$13.2^{\pm 6.3}_{\pm 1.7}$	11	$0.22^{\pm 0.11}_{\pm 0.03}$	$16.0^{\pm 7.7}_{\pm 2.1}$	$22^{\pm 10}_{\pm 3}$	0.21	14.9 ± 2.1
		$1d5/2$			$0.88^{\pm 0.42}_{\pm 0.11}$	$2.6^{\pm 1.2}_{\pm 0.3}$	–	0.83	2.85 ± 0.32
3.376	4^+	$1d5/2$	$16.7^{\pm 5.6}_{\pm 2.3}$	8	$1.42^{\pm 0.5}_{\pm 0.2}$	$2.8^{\pm 0.9}_{\pm 0.4}$	$2.8^{\pm 0.9}_{\pm 0.4}$	1.57	2.73 ± 0.35
3.576	0^+	$1d5/2$	–		–	–	–	0.28	–
3.616	2^+	$2s1/2$	$25.9^{\pm 9.0}_{\pm 3.9}$	8	$0.41^{\pm 0.14}_{\pm 0.06}$	$148^{\pm 52}_{\pm 22}$	$188^{\pm 66}_{\pm 28}$	0.35	117 ± 20
		$1d5/2$			$0.76^{\pm 0.26}_{\pm 0.11}$	$3.1^{\pm 1.1}_{\pm 0.5}$	–	0.66	2.46 ± 0.33
4.523	3^+	$2s1/2$	$41^{\pm 5}_{\pm 5}$	6	$0.84^{\pm 0.10}_{\pm 0.10}$	–	–	1.01	–

[a]Assuming the same mixing between $l = 0$ and $l = 2$ as in the mirror reaction.
[b]Assuming pure $l = 0$ for the 2^+ states and no mixing.

mirror systems, most recently determined by Al-Abdullah *et al.* [25]. In that work, the ^{17}O(^{13}C,^{12}C)^{18}O reaction was measured and ANCs for the ^{18}O bound states were extracted and then applied to the direct capture into the mirror system ^{18}Ne. Here, we apply a similar ANC analysis to the ^{18}Ne states without the need for a transformation to the mirror. The asymptotic normalization coefficients $C^2_{J,\pi}$ are extracted by matching the experimental cross section with the expression

$$\sigma = \left(\frac{C^2_{s1/2}(^{18}\text{Ne})}{b^2_{s1/2}(^{18}\text{Ne})} \sigma^{\text{CRC}}_{s1/2} + \frac{C^2_{d5/2}(^{18}\text{Ne})}{b^2_{d5/2}(^{18}\text{Ne})} \sigma^{\text{CRC}}_{d5/2} \right). \tag{1}$$

Here, the "single-particle" ANCs b_{nlj} are determined through the ratio of the single-particle-normalized, bound-state wave function of a given orbital and the corresponding Whittaker function at radii greater than 5 fm. Thus, the values of C^2 measure the overlap of the bound nuclear state with the single-particle unbound wave function outside of the nucleus. As a model for the reaction and its angular distribution we use the CRC description from the previous paragraphs, which also includes the effect of the deuteron wave function. The extracted ANC C^2 values are listed in Table II. Our results are consistent with those obtained by Al-Abdullah *et al.* [25], which are also listed.

Our results show that the 2^+_2 state contributes by far the largest ANC, owing to its being the highest excited $l = 0$ bound state. Since our experiment could not separate spectroscopic information for s and d orbits to the 2^+ states, we applied the relative contributions observed in the mirror reaction as determined in Ref. [17]. In a separate calculation, listed in Table II, we also extract the ANCs assuming that the 2^+ states were populated purely through $l = 0$ transfers. This assumption results in a difference between the extracted ANCs of less than 30%.

IV. IMPACT ON THERMAL REACTION RATES

The location and strength of the s-wave resonance at $E_R = 599.8$ keV were previously determined [5–7], and this resonance contribution dominates the ^{17}F$(p,\gamma)^{18}$Ne astrophysical rate above $T = 0.5$ GK. The results of our experiment regarding the main $l = 0$ resonance are consistent with those results within 1.4σ.

For typical nova temperatures below 0.4 GK the resonant contribution to the reaction rate from the 3^+ state at $E_R = 599.8$ keV is small compared to the direct-capture contribution. While there are no concrete expectations for a lower-energy resonance, our experiment confirms this assumption by setting upper limits on the observation of additional low-lying, strong resonances in the Gamow window.

Given the absence of additional resonances, the reaction rate for energies below 0.4 GK is dominated by the direct, bound-state capture process. This process was first analyzed by Garcia *et al.* [2], relying on spectroscopic factors from the ^{17}O$(p,\gamma)^{18}$F reaction. Subsequent works, such as that by Chipps *et al.* [7], relied on these determinations as well. The more recent determination of asymptotic normalization coefficients by Al-Abdullah *et al.* [25] also allowed for the extraction of the direct-capture rates but, again, relied on the isospin symmetry to infer the capture properties to the bound states of ^{18}Ne.

In this work, the direct-capture cross sections and the resulting astrophysical S factors for each bound state were extracted using the code RADCAP [27], relying on the asymptotic normalization coefficients from this work. We obtain a value of $S(0) = 2.44 \pm 0.97$ keV $\cdot\, b$. The corresponding direct-capture contribution to the reaction rate is listed in Table III, and displayed in Fig. 14. The upper and lower error limits on the direct capture are dominated by the statistical uncertainty in the measured ANC of the second excited 2^+ state at a level of 35%. In addition, due to the requirement of measuring γ-ray coincidences, the ground state of ^{18}Ne was not measured in this work. However, the contribution of an $l = 2$ capture to this

TABLE III. Direct-capture contribution to the rate of the $^{17}F(p,\gamma)^{18}Ne$ reaction.

Temperature	$N_A\langle\sigma v\rangle$ (cm^3 mol^{-1} s^{-1})				
(GK)	Direct[a]	Lower limit[a]	Upper limit[a]	Resonant[b]	Total
0.04	4.39×10^{-15}	2.65×10^{-15}	6.13×10^{-15}	2.31×10^{-70}	4.39×10^{-15}
0.06	2.63×10^{-12}	1.59×10^{-12}	3.67×10^{-12}	1.86×10^{-45}	2.63×10^{-12}
0.08	1.46×10^{-10}	8.84×10^{-11}	2.04×10^{-10}	4.66×10^{-33}	1.46×10^{-10}
0.1	2.53×10^{-9}	1.50×10^{-9}	3.58×10^{-9}	1.19×10^{-25}	2.53×10^{-9}
0.2	4.82×10^{-6}	2.85×10^{-6}	6.81×10^{-6}	5.37×10^{-11}	4.82×10^{-6}
0.3	1.81×10^{-4}	1.07×10^{-4}	2.56×10^{-4}	3.17×10^{-6}	1.85×10^{-4}
0.4	1.75×10^{-3}	1.04×10^{-3}	2.48×10^{-3}	6.79×10^{-4}	2.44×10^{-3}
0.5	8.75×10^{-3}	5.17×10^{-3}	1.24×10^{-2}	1.58×10^{-2}	2.46×10^{-2}
0.6	2.96×10^{-2}	1.75×10^{-2}	4.18×10^{-2}	1.22×10^{-1}	1.52×10^{-1}
0.7	7.79×10^{-2}	4.60×10^{-2}	1.10×10^{-1}	5.07×10^{-1}	5.87×10^{-1}
0.8	1.73×10^{-1}	1.02×10^{-1}	2.44×10^{-1}	1.44×10^{0}	1.61×10^{0}
0.9	3.37×10^{-1}	1.99×10^{-1}	4.76×10^{-1}	3.18×10^{0}	3.52×10^{0}

[a]From the current work.
[b]From Refs. [2] and [7].

state is expected to be small and therefore an additional, albeit nearly negligible, systematic uncertainty of 3% was included in the determination of the upper limit of the direct-capture rate. Our results for the S factor and reaction rate are slightly lower than those obtained in the calculations performed by Garcia *et al.* [2] and slightly higher than those obtained by Al-Abdullah *et al.* [25], but within errors consistent with both.

V. SUMMARY

We performed an experiment with the $^{17}F(d,n)^{18}Ne$ reaction in inverse kinematics, using a beam of the radioactive isotope ^{17}F at 5.62 A MeV, produced with the RESOLUT radioactive-ion-beam facility at the John D. Fox Accelerator Laboratory of Florida State University. The experiment with the compact RESONEUT detector system allowed for the coincident detection of neutrons, protons, γ rays, and heavy ions. Spectroscopy of protons emitted after the population of ^{18}Ne resonances was used to determine the total population cross section for the main $l = 0$ resonances, the 3^+ at 0.598-MeV c.m. resonance energy and the 2^+ at 1.17 MeV. Through comparison with a CRC calculation of the total transfer cross section, the spectroscopic factors for the 3^+ and 2^+ resonances were extracted and the proton widths were deduced. Both extracted spectroscopic factors are consistent with those obtained from $^{17}O(d,p)^{18}O$ experiments. In addition, the deduced proton widths differ only slightly from the proton widths measured in the proton elastic scattering experiments. These results shows that the analysis of (d,n) transfer reactions can be used to obtain quantitative results about astrophysical reaction rates.

The experimental setup with a compact system of 10 neutron detectors also allowed for neutron time-of-flight spectroscopy, the first time this technique has been successfully implemented in a (d,n) reaction and a radioactive ion beam experiment. The neutron spectrum showed the population of the $l = 0$ (3^+) resonance at $E_R = 0.60$ MeV, as well as the population of the 2^+_1, 4^+_1, and 2^+_2 bound states in ^{18}Ne. We extracted asymptotic normalization coefficients for these bound states, which were analyzed to extract the astrophysical S factor associated with direct capture, the dominant mechanism for the astrophysical $^{17}F(p,\gamma)^{18}Ne$ reaction at temperatures below 0.4 GK. The results of our experiment are consistent with prior analyses, which used a theoretical translation of experimental information obtained in isospin-mirror systems. This experiment for the first time determines the direct-capture component of the $^{17}F(p,\gamma)^{18}Ne$ reaction from experimental information on ^{18}Ne.

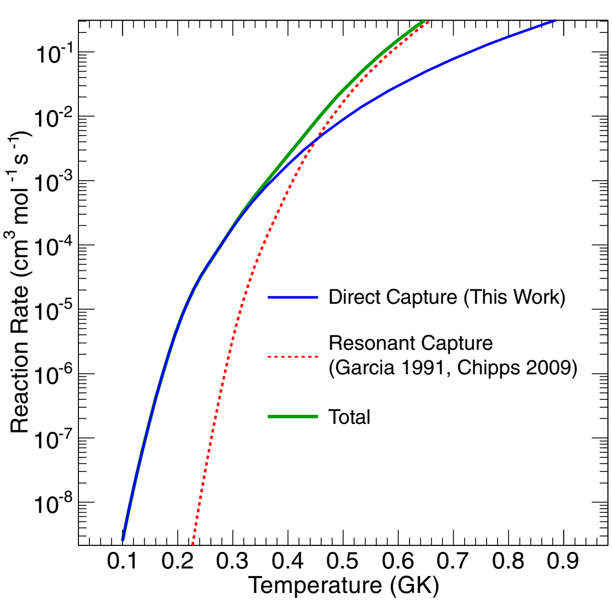

FIG. 14. Direct-capture reaction rate calculated using the ANCs measured in this work and the calculated astrophysical S factors.

ACKNOWLEDGMENTS

This work was partially supported by the National Science Foundation, under Grant Nos. PHY-1401574, PHY-1064819, and PHY-1126345 and partially supported by the U.S. Department of Energy, Office of Science, under Grant Nos. DE-FG02-02ER41220 and DE-FG02-96ER40978.

[1] M. Wiescher, J. Görres, E. Uberseder, G. Imbriani, and M. Pignatari, The cold and hot CNO cycles, Annu. Rev. Nucl. Part. Sci. **60**, 381 (2010).

[2] A. García, E. G. Adelberger, P. V. Magnus, D. M. Markoff, K. B. Swartz, M. S. Smith, K. I. Hahn, N. Bateman, and P. D. Parker, The "missing" 3^+ state of ^{18}Ne and explosive ^{17}F(p,γ) burning, Phys. Rev. C **43**, 2012 (1991).

[3] S. H. Park, S. Kubono, K. I. Hahn, C. S. Lee, J. C. Kim, P. Strasser, S. C. Jeong, M. H. Tanaka, C. Lee, J. H. Lee, S. Kato, T. Miyachi, H. Kawashima, H. Utsunomiya, M. Yasue, M. Kurokawa, Y. Fuchi, X. Liu, K. Abe, K. Kumagai, M. S. Smith, and P. D. Parker, High-resolution study of the ^{18}Ne excited states relevant to the hot CNO cycle, Phys. Rev. C **59**, 1182 (1999).

[4] Y. Parpottas, S. M. Grimes, S. Al-Quraishi, C. R. Brune, T. N. Massey, J. E. O'Donnell, J. E. Oldendick, A. Salas, and R. T. Wheeler, The ^{17}F$(p,\gamma)^{18}$Ne3^+ resonance state studied with the ^{16}O(^{3}He, n)^{18}Ne reaction, Phys. Rev. C **72**, 025802 (2005).

[5] D. W. Bardayan, J. C. Blackmon, C. R. Brune, A. E. Champagne, A. A. Chen, J. M. Cox, T. Davinson, V. Y. Hansper, M. A. Hofstee, B. A. Johnson, R. L. Kozub, Z. Ma, P. D. Parker, D. E. Pierce, M. T. Rabban, A. C. Shotter, M. S. Smith, K. B. Swartz, D. W. Visser, and P. J. Woods, Observation of the Astrophysically Important 3^+ State in ^{18}Ne via Elastic Scattering of a Radioactive ^{17}F Beam from ^{1}H, Phys. Rev. Lett. **83**, 45 (1999).

[6] D. W. Bardayan, J. C. Blackmon, C. R. Brune, A. E. Champagne, A. A. Chen, J. M. Cox, T. Davinson, V. Y. Hansper, M. A. Hofstee, B. A. Johnson, R. L. Kozub, Z. Ma, P. D. Parker, D. E. Pierce, M. T. Rabban, A. C. Shotter, M. S. Smith, K. B. Swartz, D. W. Visser, and P. J. Woods, The astrophysically important 3^+ state in ^{18}Ne and the ^{17}F$(p,\gamma)^{18}$Ne stellar rate, Phys. Rev. C **62**, 055804 (2000).

[7] K. A. Chipps, D. W. Bardayan, J. C. Blackmon, K. Y. Chae, U. Greife, R. Hatarik, R. L. Kozub, C. Matei, B. H. Moazen, C. D. Nesaraja, S. D. Pain, W. A. Peters, S. T. Pittman, J. F. Shriner, and M. S. Smith, First Direct Measurement of the ^{17}F$(p,\gamma)^{18}$Ne Cross Section, Phys. Rev. Lett. **102**, 152502 (2009).

[8] P. N. Peplowski, L. T. Baby, I. Wiedenhöver, S. E. Dekat, E. Diffenderfer, D. L. Gay, O. Grubor-Urosevic, P. Höflich, R. A. Kaye, N. Keeley, A. Rojas, and A. Volya, Lowest $l = 0$ proton resonance in ^{26}Si and implications for nucleosynthesis of ^{26}Al, Phys. Rev. C **79**, 032801 (2009).

[9] J. Baker, *Experimental Study of the Proton Capture on Al-25 Using the* ^{25}Al$(d,n)^{26}$Si *Reaction in Inverse Kinematics*, Ph.D. thesis, Florida State University (2016).

[10] A. S. Adekola, C. R. Brune, D. W. Bardayan, J. C. Blackmon, K. Y. Chae, J. A. Cizewski, K. L. Jones, R. L. Kozub, T. N. Massey, C. D. Nesaraja, S. D. Pain, J. F. Shriner, M. S. Smith, and J. S. Thomas, ^{19}Ne levels studied with the ^{18}F$(d,n)^{19}$Ne*(^{18}F + p) reaction, Phys. Rev. C **85**, 037601 (2012).

[11] J. Belarge, S. A. Kuvin, L. T. Baby, J. Baker, I. Wiedenhöver, P. Höflich, A. Volya, J. C. Blackmon, C. M. Deibel, H. E. Gardiner, J. Lai, L. E. Linhardt, K. T. Macon, E. Need, B. C. Rasco, N. Quails, K. Colbert, D. L. Gay, and N. Keeley, Experimental Investigation of the ^{19}Ne$(p,\gamma)^{20}$Na Reaction Rate and Implications for Breakout from the Hot CNO Cycle, Phys. Rev. Lett. **117**, 182701 (2016).

[12] L. T. Baby, S. Kuvin, I. Wiedenhöver, M. Anastasiou, D. Caussyn, K. Colbert, N. Quails, and D. Gay, Resoneut: A detector system for spectroscopy with (d,n) reactions in inverse kinematics, Nuclear. Instr. and Phys. Res., Sec. **877**, 34–43 (2018).

[13] I. Wiedenhöver, L. T. Baby, D. Santiago-Gonzalez, A. Rojas, J. C. Blackmon, G. V. Rogachev, J. Belarge, E. Koshchiy, A. N. Kuchera, L. E. Linhardt, J. Lail, K. T. Macon, M. Matos, and B. C. Rascol, *Studies of Exotic Nuclei at the RESOLUT Facility of Florida State University* (World Scientific, Singapore, 2013), pp 144–151.

[14] J. Lai *et al.* (unpublished).

[15] N. I. Kaloskamis, K. C. Chan, A. A. Chishti, J. S. Greenberg, C. J. Lister, S. J. Freedman, M. Wolanski, J. Last, and B. Utts, The trigger detector for APEX: An array of position-sensitive NaI(Tl) detectors for the imaging of positrons from heavy-ion collisions, Nucl. Instrum. Methods Phys. Res., Sec. A **330**, 447 (1993).

[16] B. C. Perry, C. M. Campbell, J. A. Church, D.-C. Dinca, J. Enders, T. Glasmacher, Z. Hu, K. L. Miller, W. F. Mueller, and H. Olliver, A high-efficiency NaI(Tl) detector array with position sensitivity for experiments with fast exotic beams, Nucl. Instrum. Methods Phys. Res., Sec. A **505**, 85 (2003).

[17] T. K. Li, D. Dehnhard, Ronald E. Brown, and P. J. Ellis, Investigation of the $(d_{\frac{5}{2}})^2$ and $(d_{\frac{5}{2}} s_{\frac{1}{2}})$ two-particle configurations in ^{18}O using the ^{17}O$(\vec{d},p)^{18}$O reaction at 18 MeV, Phys. Rev. C **13**, 55 (1976).

[18] S.-J. Jin, Y.-B. Wang, B.-X. Wang, X.-X. Bai, X. Fang, B. Guo, E.-T. Li, Y.-J. Li, Z.-H. Li, G. Lian, J. Su, S.-Q. Yan, S. Zeng, Z.-E. Yao, and W.-P. Liu, Excited states in ^{18}Ne studied via ^{17}F + p, Chin. Phys. Lett. **27**, 032102 (2010).

[19] I. J. Thompson, Coupled reaction channels calculations in nuclear physics, Comput. Phys. Rep. **7**, 167 (1988).

[20] A. J. Koning and J. P. Delaroche, Local and global nucleon optical models from 1 keV to 200 meV, Nucl. Phys. A **713**, 231 (2003).

[21] R. V. Reid, Local phenomenological nucleon-nucleon potentials, Ann. Phys. **50**, 411 (1968).

[22] G. H. Rawitscher, Effect of deuteron breakup on (d,p) cross sections, Phys. Rev. C **11**, 1152 (1975).

[23] N. Keeley, N. Alamanos, and V. Lapoux, Comprehensive analysis method for (d,p) stripping reactions, Phys. Rev. C **69**, 064604 (2004).

[24] D. R. Tilley, H. R. Weller, C. M. Cheves, and R. M. Chasteler, Energy levels of light nuclei $a = 18$–19, Nucl. Phys. A **595**, 1 (1995).

[25] T. Al-Abdullah, F. Carstoiu, X. Chen, H. L. Clark, C. A. Gagliardi, Y.-W. Lui, A. Mukhamedzhanov, G. Tabacaru, Y. Tokimoto, L. Trache, R. E. Tribble, and Y. Zhai, Astrophysical reaction rate for ^{17}F$(p,\gamma)^{18}$Ne from the transfer reaction ^{13}C(^{17}O,^{18}O)^{12}C, Phys. Rev. C **89**, 025809 (2014).

[26] R. E. Tribble, C. A. Bertulani, M. La Cognata, A. M. Mukhamedzhanov, and C. Spitaleri, Indirect techniques in nuclear astrophysics: A review, Rep. Prog. Phys. **77**, 106901 (2014).

[27] C. A. Bertulani, Radcap: A potential model tool for direct capture reactions, Comput. Phys. Commun. **156**, 123 (2003).